Research article

Cholesterol recognition motifs in the transmembrane domain of the tyrosine kinase receptor family: the case for TRKB

Cecilia Cannarozzo[1], Senem Merve Fred[1], Mykhailo Girych[2], Caroline Biojone[1], Giray Enkavi[2], Tomasz Róg[2], Ilpo Vattulainen[2,3], Plinio C Casarotto[1]*, Eero Castrén[1]

1: Neuroscience Center - HiLIFE, University of Helsinki, Finland.

2: Department of Physics, University of Helsinki, Finland.

3: Computational Physics Laboratory, Tampere University, Finland.

* corresponding author: Plinio Cabrera Casarotto, PhD. Neuroscience Center. Haartmaninkatu 8, B233b. PO Box 63. University of Helsinki, Finland. plinio.casarotto@helsinki.fi

ABSTRACT

Cholesterol is an essential constituent of cell membranes. Recently, the discovery of cholesterol recognition amino acid consensus (CRAC) on proteins indicated a putative direct, non-covalent interaction between cholesterol and proteins. In the present study, we evaluated the presence of a CRAC motif and its inverted version (CARC) in the transmembrane region (TMR) of the tyrosine kinase receptor family (RTK) in several species using *in silico* methods. CRAC motifs were found across all species analyzed, while CARC was found only in vertebrates. The tropomyosin-related kinase B (TRKB), a member of the RTK family, is a core participant in the neuronal plasticity process and exhibits a CARC motif in its TMR. Upon recognition of the conserved CARC motif in the TRKB, we compared the effect of point mutations in CARC on structural changes in the TMR of mouse TRKB. The alignment of wild-type and mutant TMR indicates small morphological changes across the 6 mutations analyzed (Y433F, Y433C, Y433A, V437K, R427A, and the double mutation R427A/Y433F), as demonstrated by the root-mean-squared deviation values for the superimposed structures. A molecular dynamics simulation with the mouse TRKB TMR sequence indicated that cholesterol interaction with the TRKB CARC motif is reduced by the R427A/Y433F mutation. Experimental data assayed by fluorescence recovery after photobleaching indicated a reduction in brain-derived neurotrophic factor-induced mobility of TRKB.R427A/Y433F in the spine of cultured hippocampal neurons. Therefore, CARC/CRAC motifs may have a role in the function of the RTK family TMR.

Keywords: cholesterol-recognition motif, TRKB, tyrosine kinase family, BDNF

INTRODUCTION

The human brain contains 23% of the body's total cholesterol. Most of this cholesterol is found in the myelin sheath of oligodendrocytes (Dietschy and Turley 2004; Martin et al. 2014). As the blood-brain barrier prevents lipoprotein or cholesterol transport to the brain, local *de novo* synthesis takes place. In the mouse brain, cholesterol synthesis peaks during the second postnatal week and then decreases significantly independent of sex or blood cholesterol concentration (Quan et al. 2003; Pfrieger and Ungerer 2011). During early development, neurons produce cholesterol autonomously (Chaves et al. 1997; Nieweg et al. 2009; Pfrieger and Ungerer 2011). In later stages, cholesterol is synthesized by glial cells. However, it is unknown if this synthesis is constant or under regulated production (Saito et al. 2009; Pfrieger and Ungerer 2011).

Cholesterol can be localized on both leaflets of the plasma membrane (Fantini et al. 2016) and induces changes in physical properties of the membrane, such as fluidity (Maguire and Druse 1989) and curvature (Lee 2004). Cholesterol can also interact with transmembrane domains to regulate protein function (Fantini and Barrantes 2013; Elkins et al. 2018). Cholesterol is a core constituent of microdomains known as lipid rafts, which serve as signaling platforms for several pathways (Lang et al. 2001; Pereira and Chao 2007; Zonta and Minichiello 2013). In the nervous system, cholesterol interaction with membrane proteins influences several crucial events, such as exocytosis of synaptic vesicles (Linetti et al. 2010), synaptic activity, connectivity, plasticity, signal transduction, transmission, and cell survival (Michikawa and Yanagisawa 1999; Goritz et al. 2005; Liu et al. 2010).

The tropomyosin-related kinase receptor (TRK) subfamily is one of the most prominent subfamilies of tyrosine kinase receptors (RTK) and plays a crucial role in neuronal plasticity (Dekkers et al. 2013). The TRK receptors consist of three members (TRKA, TRKB, and TRKC) that are phosphorylated on different tyrosine residues on the intracellular portion upon activation by their high-affinity ligands (NGF, BDNF, and NT-3, respectively) (Huang and Reichardt 2001). TRKA and TRKC (NTRK1 and NTRK3, respectively) are located in lipid rafts, while the presence of TRKB (NTRK2) in rafts occurs upon BDNF stimulation (Suzuki et al. 2004, 2007). Functionally, in the absence of ligand, TRKA and TRKC (but not TRKB) induce cell death mediated by interaction with p75NTR, the low-affinity receptor of several neurotrophins (Dekkers et al. 2013).

In silico models suggest that two cholesterol molecules can interact in a tail-to-tail fashion as a transbilayer dimer (Harris et al. 1995; Rukmini et al. 2001) or back-to-back through their flat alpha faces, leaving the beta sides accessible for interactions with proteins (Hanson et al. 2008). On these target proteins, the following two consensus motifs with predictive value have been defined (Di Scala et al. 2017): the Cholesterol Recognition Amino acid Consensus sequence (CRAC) and its "inverted" version (CARC) (Li and Papadopoulos 1998; Baier et al. 2011). The CRAC linear sequence, from N- to C-terminus, consists of an apolar residue (leucine [L] or valine [V]), one to five amino acids of any kind, an aromatic amino acid (tyrosine [Y] or phenylalanine [F]), one to five amino acids of any kind, and a basic residue (arginine [R] or lysine [K]) (Fantini and Barrantes 2013). CARC consists of the same pattern in the opposite direction, with tryptophan (W) as alternative aromatic residue. CARC has a higher affinity for cholesterol than CRAC (Fantini and Barrantes 2013; Di Scala et al. 2017). Several proteins have been identified to contain CRAC/CARC motifs, such as nicotinic acetylcholine (nAchR), type-3 somatostatin, and GABA-A receptors (Jamin et al. 2005; Epand 2006; Fantini and Barrantes 2013).

The aim of the present study was to evaluate the incidence of cholesterol-interacting motifs (CRAC and CARC) in the RTK family. Given the promiscuous nature of CRAC motifs, we focused on the RTK transmembrane region (TMR; transmembrane domain plus the 5-amino acid flanking residues on both N-

and C-terminal sides), where such interaction has a higher probability of occurrence. Transmembrane domains are crucial for proper positioning in the lipid bilayer of biological membranes (Fantini and Barrantes 2013). Interaction of transmembrane domains of embedded integral proteins with the lipid component of the bilayer provides a diffusion barrier and encloses the environment to maintain electrochemical properties (Hunte 2005). Upon identification of CARC in TRKB TMR (but not in TRKA or TRKC), we assessed the impact of a series of mutations on the interaction of the transmembrane region with cholesterol (as measured by molecular dynamic simulations) and on conformation in mouse TRKB.TMR. Finally, we evaluated the impact of a mutation in the CARC motif on BDNF-induced movement of TRKB in the spines of hippocampal neurons.

METHODS

Data mining

For data mining, we used 144 hand-curated inputs of RTK family (code 2.7.10.1) from the UniProt database (The UniProt Consortium 2017). The canonical primary structure of TMR (transmembrane domain and the flanking 5 amino acid residues, from N- and C-terminal) of RTK from each target of human (52 proteins), mouse (51 proteins), zebrafish (14 proteins), fruit fly (12 proteins), and nematode *C. elegans* (15 proteins) databases were extracted. The TMR FASTA sequences for each protein were manually screened for the presence of cholesterol recognition alignment consensus, both CRAC and CARC (Fantini and Barrantes 2013; Fantini et al. 2016). We then searched for putative pathogenic mutations in human proteins using SwissVar, ClinVar, and COSMIC databases (Mottaz et al. 2010; Landrum et al. 2018; Tate et al. 2019).

Percentage of identity of TRKB (and TMR) across species

The Percentage Identity (PI) of TRKB.TMR (and full-length sequences) among several species, including *D. rerio* (zebrafish), *G. gallus* (chicken), *C. familiaris* (dog), *R. norvegicus* (rat), *M. musculus* (mouse), *P. troglodytes* (chimpanzee), and *H. sapiens* (human), was determined using the align tool in UniProt database (The UniProt Consortium 2017). The correlation between PI in full-length TRKB and TRKB.TMR among the different species was determined by Spearman's test (GraphPad Prism v.6.07). The PI trees for full TRKB and TMR.TRKB were obtained using the tree tool (Neighbour Joining, BLOSUM62) in Jalview v.2.0 software (Waterhouse et al. 2009).

Alignment of the models

The models of mouse TRKB.TMR (in this case with extra 10 amino acid residues in each terminal) were generated in the RaptorX server (Källberg et al. 2012) using wild-type (WT) and mutated FASTA sequences. The point mutation Y433F was chosen to exclude only the -OH group but protected the aromatic ring structure of tyrosine. The Y433A mutation was introduced to examine the effects of removing the aromatic ring of tyrosine. Finally, the Y433C mutation was introduced based on evidence showing the association of this particular change with hyperphagic obesity syndrome (Y434 in human TRKB), which also causes defective memory and learning, as well as developmental and epileptic encephalopathy (Yeo et al. 2004; Hamdan et al. 2017). The V437K mutation was chosen to change an apolar/neutral residue to a basic residue; the same rationale was considered for the R427A mutation. Finally, the impact of the double R427A/Y433F mutation was analyzed. The models were aligned with WT and the root-mean-squared deviation (RMSD) between the backbone carbon structure was calculated by the server.

Molecular dynamics simulations

The 3-dimensional (3D) structure of the TMR of TRKB (residues 423-460) was generated using the FMAP

(Folding of Membrane-Associated Peptides) server (Lomize et al. 2018). The server predicted that the residues V432-A456 form an α-helical transmembrane segment; the remaining sequence is unstructured. This structure was used as an atomistic model for the TRKB.wt (wild type) and TRKB.mut (R427A/Y433F) proteins. For coarse-grained simulations, these atomistic structures were used as the basis. For this purpose, all protein-membrane systems were constructed using the CHARMM-GUI Martini Maker (Hsu et al. 2017), where the TRKB.wt and TRKB.mut were separately embedded in a bilayer (512 lipids) composed of 60 mol% palmitoyl-oleoyl-phosphatidylcholine (POPC) and 40 mol% cholesterol. Each system was solvated with 6038 water beads (approximately 50 water molecules per lipid). Sodium and chloride ions were added to reach 0.15 M salt concentration and to neutralize the system.

All simulations were performed using Gromacs 5.1.4 (Abraham et al. 2015) employing the non-polarizable Martini 2.2 force field for the protein (de Jong et al. 2013) and lipids (Arnarez et al. 2015). The simulations were performed using the "New-RF" parameters (de Jong et al. 2016). For electrostatics, the reaction field method was used with a cutoff of 1.1 nm. Lennard-Jones interactions were cut off at 1.1 nm. The potential shift modifier was applied to non-bonded interactions together with buffered Verlet lists (Páll and Hess 2013). The equations of motion were integrated using the leap-frog algorithm with a 25-fs time step. The simulations were performed at 310 K in the NpT ensemble at a pressure of 1 bar. The protein, the membrane, and the solvent (water and 0.15 M NaCl) were coupled to separate heat baths with a time constant of 1.0 ps using the V-rescale thermostat (Bussi et al. 2007). Pressure was controlled semi-isotropically using the Parrinello-Rahman barostat (Parrinello and Rahman 1981) with a time constant of 12 ps and a compressibility of 3×10^{-4} bar^{-1} in the xy-plane (membrane plane). The systems were first equilibrated with the protein backbone atoms restrained. In the production stage, each system (TRKB.wt and TRKB.mut) was simulated for 5 μs through 9 independent repeats.

All analyses were performed using the Gromacs software package and in-house scripts, using only the last 4 μs of the simulations. The data presented (figure 3g) is the average occupancy of cholesterol (occupancy) that represents the average number of cholesterol molecules within 0.6 nm of the alpha carbon (MARTINI backbone bead) at residue positions 427 and 433. The occupancy values are produced by dividing the total number of contacts by the number of frames in each trajectory.

Cell cultures and fluorescence recovery after photobleaching

Hippocampal cells from rat embryo (E18; DIV16-18) were cultivated onto glass coverslips coated with poly-L-lysine at 200 000 cells/well (Sahu et al. 2019). The cultures were maintained at 37ºC in serum-free Neurobasal medium (supplemented with 2% B27, 1% L-glutamine, and 1% ampicillin) and transfected by calcium phosphate co-precipitation method (Xia et al. 1996) to overexpress GFP-tagged TRKB constructs from mouse sequence (TRKB.WT or TRKB.R427A/Y433F). Fluorescence recovery after photobleaching (FRAP) was performed with a confocal microscope (Zeiss LSM 710, Carl Zeiss AG) at 37ºC and 5% CO_2. Coverslips with the cultured hippocampal neurons were transferred to 35-mm Petri dishes with phenol- and serum-free HBSS medium. Dendritic shafts or spines (spine head diameter = ~1 μm) were localized with a 63x/0.90 NA dipping water objective (Koskinen et al. 2012). Three frames were taken from the region of interest (ROI) for the normalization (prebleaching), setting the first frame as 100% FRAP start value. The bleaching phase consisted of a short cycle (1-5 bleach iterations, approximately 0.01-0.5 s) of bleaching to decrease the signal of the ROI to 50%. The postbleaching phase lasted for 2 minutes (with a time resolution of 2s/frame) until a plateau was reached and the shape of the recovery curve was clear. Next, BDNF (20 ng/ml) was added to the medium for 15 minutes. After establishing the baseline, bleaching was performed in different dendritic shafts or spines and the following recording lasted again for 2 minutes (time resolution of 2s/frame). Once added to the medium, BDNF was present for the remainder of the FRAP recording. The

intensity value of the bleached ROI was normalized to a second neighboring unbleached dendritic ROI of the same area and of similar initial intensity to compensate for the photobleaching generated in the acquisition of the images. This intensity value was then converted to percentage by dividing the intensity values of individual frames by the start value of the first frame (t0=100%). The mean values from the different experimental groups were plotted along the 2-minute recording to generate the recovery curve (González-González et al. 2012; Koskinen et al. 2012; Casarotto et al. 2019). The data was analyzed by two-way ANOVA with repeated measures, with treatment (BDNF vs ctrl) and fluorescence along time as factors using GraphPad Prism v.6.07.

RESULTS

Data mining

The presence of CRAC motifs was found throughout all the species analyzed (human, 11 of 52 proteins; mouse, 10 of 51 proteins; zebrafish, 2 of 14 proteins; fruit fly, 2 of 12 proteins; and *C. elegans*, 2 of 15 proteins, figure 1). However, the presence of CARC motifs in the RTK family was observed only in vertebrates, with 3 in human, 3 in mouse, and 2 in zebrafish RTK. None of the proteins analyzed was found to carry CRAC and CARC motifs simultaneously. The ClinVar and COSMIC databases indicated five proteins (Table 1) consisting of 8 mutations in the CRAC/CARC domains associated with central nervous system or endocrine disorders or cancer.

The full list of proteins positive to CRAC/CARC is found in table 1 and the full list of proteins examined from each species can be found in the deposited raw data (DOI:10.6084/m9.figshare.7935980).

Percentage of identity of TRKB (and TMR) across species

Upon identification of the CARC motif in TRKB (human and mouse, REHLSVYAVVV; zebrafish, RVAVYIVV), the PI between TRKB.TMR sequences of several species (human, chimpanzee, mouse, rat, dog, chicken, and zebrafish; table 2) was examined using UniProt(The UniProt Consortium 2017). Over 90% PI was found in both TRKB.TMR and full-length TRKB of human, chimpanzee, mouse, rat, and dog. The PI results of paired comparison between the species analyzed are organized in figure 2, where the green gradient highlights the percentage similarity between the sequences. For comparative purposes, we also determined the PI of full-length TRKB among these species. The PI results of paired comparisons are also organized in figure 2, with red gradient highlighting similarity. Spearman's test indicated a significant correlation between the full-length TRKB and TRKB.TMR (R^2= 0.8530, 99% confidence interval [CI] = 0.8135-0.9698; $p<0.0001$).

Alignment of the models

We proceeded with mouse TRKB.TMR to analyze the impact of point mutations on arginine, tyrosine, or valine in the structure of this region. The mutations induced small morphological changes when the wild-type and mutant models were aligned, as indicated by the RMSD values (figure 3). TRKB TMR RMSD (Å) values were as follows: Y433F=1.990; Y433C=2.310; Y433A=2.290; V438K=2.380; R427A=2.990; R428/Y433Y= 3.030.

Molecular dynamics simulations

To study the effect of the R427A/Y433F mutation on the interaction between cholesterol and TRKB TMR, we performed coarse-grained simulations of the TMR of wildtype (TRKB.wt) and the double mutant (TRKB.mut) embedded in a 40 mol% cholesterol bilayer. Analysis of the trajectories in terms of average

cholesterol occupancy (see Methods) revealed that the R427A/Y433F mutation results in a substantial and significant decrease [genotype effect: $F(1,32)=123.5$, $p<0.0001$, n=9/group] in the average occupancy of cholesterol molecules in the vicinity of the TRKB CARC domain (figure 3g). Specifically, the double mutant caused a 47% and 23% decrease in cholesterol occupancy in the vicinity of mutant residues 427 and 433, respectively.

Fluorescence recovery after photobleaching

The analysis by two-way ANOVA with repeated measures indicated a significant effect of BDNF treatment over time in cells transfected with TRKB.wt [interaction: $F(69,3036)=3.458$, $p<0.0001$, n=25,21] but not in those transfected with TRKB.mut [interaction $F(69,3243)=0.878$, $p=0.754$, n=26,23]. As previously observed (Casarotto et al. 2019), administration of BDNF recovered the fluorescence in the spine of cells transfected with GFP-tagged TRKB (figure 4c-h). However, the mutation in the TRKB CARC motif impaired such an effect of BDNF (figure 4).

DISCUSSION

In the present study, we evaluated the incidence of cholesterol-recognition motifs in the RTK family from mouse, human, zebrafish, fruit fly, and the nematode *C. elegans*. We found that while the *bona fide* CRAC, located in the C-terminal portion of the transmembrane domain (Fantini and Barrantes 2013), is found in all species analyzed, its inverted version (CARC) was observed only in vertebrates. Furthermore, we found that TRKB, a tyrosine-kinase receptor crucial for neuronal plasticity, contains a CARC sequence in the TMR that is conserved across different species. However, CRAC/CARC motifs were absent in the TMR of other members of the TRK subfamily, such as TRKA and TRKC.

Cholesterol can interact with membrane proteins in several ways. One of its most prominent effects involves a direct post-translational modification on members of the Hedgehog pathway; this has been described in *Drosophila sp.* (Jeong and McMahon 2002; Wendler et al. 2006). In this model organism, cholesterol also regulates membrane depolarization through transient receptor potential (TRP) channels (Peters et al. 2017) and serves as a precursor for ecdysteroids, which in turn control several steps of fly development (Niwa and Niwa 2014). In nematodes such as *C. elegans*, cholesterol is only obtained from diet, although these worms can modify the basic steroid structure into derivatives (Kurzchalia and Ward 2003). In both organisms, cholesterol appears to play a major role as a signaling molecule with post-translational modifications of proteins as the main mechanism (Mann and Beachy 2000).

In vertebrates, although neurons synthesize the absolute minimum of required cholesterol, glial production and release of lipoproteins supply neuronal demand during development and in adulthood (Mauch et al. 2001). In particular, apolipoprotein E (APOE) is synthesized primarily by astrocytes and glial cells (Boyles et al. 1985; Pfrieger and Ungerer 2011). Glia-derived cholesterol stimulates synapse formation and synaptic efficacy (Pfrieger 2003b, a). In the presynaptic plasma membrane, cholesterol-rich lipid rafts are necessary for SNARE-dependent exocytosis of vesicles with high cholesterol content. At the postsynaptic level, such rafts organize the disposition of receptors, protein scaffolds, and signaling cascades (Pfrieger 2003b, a). Importantly, cholesterol removal from neuronal cultures impairs exocytosis of synaptic vesicles(Linetti et al. 2010), synaptic transmission (Goritz et al. 2005), and neuronal viability (Michikawa and Yanagisawa 1999). In addition, cholesterol induces clustering of AMPA receptors and hinders NMDA-induced long-term potentiation in the hippocampus (Frank et al. 2008; Martín et al. 2014).

Two consensus motifs with predictive value for cholesterol interaction with proteins have been defined through *in silico* methods (Di Scala et al. 2017) in CRAC and CARC (Li and Papadopoulos 1998; Baier et al.

2011). The non-covalent binding of cholesterol to such motifs has been the focus of various recent studies. For example, cholesterol modulates docking of NMDA receptors into lipid rafts (Korinek et al. 2015) and the function of vanilloid receptors TRPV1, a member of the TRP family (Jansson et al. 2013), thus interfering in synaptic plasticity. Increased cholesterol concentration enhances the plasticity and flexibility of 5HT1a dimers and adrenergic receptors (Prasanna et al. 2014, 2016). Given the opposed dispositions of CARC and CRAC motifs, it is possible to assume the co-existence of both in the same transmembrane domain and their potential interaction with two cholesterol molecules in a tail-to-tail configuration (Di Scala et al. 2017). However, none of the analyzed TMR of RTK family members in the present study displayed co-existing CARC and CRAC motifs.

Interestingly, we only observed the occurrence of CARC motifs in the zebrafish, mouse, and human RTK family. TRKB.TMR is highly conserved among vertebrates, similar to full-length TRKB. However, the TRKB.TMR CARC sequence from chicken differs in the juxtamembrane residue from the other species compared here (table 2). The following two scenarios are plausible. The role of R/K (charged, basic residues) is fulfilled by glutamate (E), which is also charged at pH 7, although negatively, or by asparagine (N), which is not charged but carries a basic amino group. Additionally, for the second possibility it is also necessary to relax the proposed "5-residue rule" between the Y and the juxtamembrane residue (Fantini et al. 2019), since N is located 6 residues apart from the central Y. Although correlated, the PI of full-length TRKB and TRKB.TMR are not comparable. Given the large difference in the number of residues between these two sequences, each residue change in the TMR exerts a higher impact than on full-length TRKB in the overall PI between the species analyzed.

As mentioned above, TRKB plays a crucial role in several aspects of neuronal plasticity (Park and Poo 2013). The activation of this receptor is associated with the reopening of visual critical period(Maya Vetencourt et al. 2008) and the formation, retention, and recall of memory (Karpova et al. 2011; Bekinschtein et al. 2014). Increased TRKB activity is linked to the occurrence of epilepsy, while blockade of such signaling normalizes the condition (Heinrich et al. 2011; Liu et al. 2013). Whole-genome sequencing performed on patients with developmental and epileptic encephalopathy linked a *de novo* missense variant of TRKB (*NTRK2*) to the disease pathology (Hamdan et al. 2017). Patients carrying cysteine at residue 434 instead of tyrosine, located inside the TRKB CARC motif, have a similar phenotype varying from severe global developmental delay or intellectual disability to visual and feeding impairments (Hamdan et al. 2017). Therefore, it is possible that such a Y434C mutation, which interferes with TRKB-cholesterol interaction, leads to dysregulated TRKB activity and function.

Neurotrophins induce homodimerization of TRK monomers to activate downstream kinases (Bothwell 2014). However, through a p75NTR-dependent mechanism, TRKA and TRKC receptors may induce cell death in the absence of their ligands (NGF or NT-3, respectively). On the other hand, TRKB does not act as a death-inducing receptor in the absence of BDNF (Nikoletopoulou et al. 2010). It has been suggested that TRKA and TRKC interaction with p75NTR is a necessary step for moving the complex to lipid rafts, where the p75NTR-dependent death signal is triggered through its cleavage by gamma secretase (Dekkers et al. 2013). TRKB did not exhibit such co-occurrence with p75NTR in lipid rafts. The association of TRKA and TRKC with p75NTR in rafts involves the transmembrane domain of these receptors, given that a chimeric TRKB carrying TRKA transmembrane sequence requires BDNF for survival signal (Dekkers et al. 2013). Curiously, p75NTR possesses a classical CRAC domain in its TMR (VVVGLVAYIAFKR) that is conserved in the human, mouse, and rat.

According to *in silico* analysis of cholesterol interaction with CARC motifs, the Y to F or Y to W mutations should not interfere with the motif interaction with cholesterol. However, these analyses were performed in

multipass or multi-subunits transmembrane receptors, such as nicotinic cholinergic (Di Scala et al. 2017) or GPCR receptors (Prasanna et al. 2014, 2016). Given that TRKB and virtually all members of the RTK family possess a single transmembrane domain, small changes in this region may impact their function but remain undetected in the multipass proteins or in the direct interaction with cholesterol. Consistent with this, our simulations indicate that cholesterol interaction with CARC motif is decreased in mutant TRKB.

The substantial decrease of cholesterol occupancy near the TRKB CARC domain due to the double mutation observed in our simulations is consistent with our recent study that included mouse TRKB.Y433F (Casarotto et al. 2019). In this study, the TRKB.Y433F mutation compromised the ability of BDNF to induce TRKB clustering and its recruitment in cholesterol-enriched membrane domains as revealed by direct stochastic optical reconstruction and FRAP, respectively. In the present study, the double mutation in the CARC motif of TRKB (R427A/Y433F) showed a similar effect.

TRKB is found in lipid rafts only upon activation by BDNF (Suzuki et al. 2004). Interestingly, when cholesterol is sequestered, TRKB translocation to lipid rafts is impaired, and BDNF-dependent potentiation is prevented (Suzuki et al. 2004). However, loss of cholesterol in hippocampal cultures is associated with increased baseline activity of TRKB (Martin et al. 2008). These opposite outcomes might be due to a differential modulation exerted by cholesterol, depending on the challenge to TRKB receptor (basal vs BDNF-stimulated), cell type or origin, and stage of differentiation. Another possibility is that cholesterol affects TRKB activity in a bell-shaped manner, where higher and lower cholesterol concentrations impede instead of promote TRKB phosphorylation. In fact, the decrease of cholesterol levels by beta-cyclodextrin was found to differentially modulate neurite growth of hippocampal and cortical cultured neurons (Ko et al. 2005). In hippocampal cells, the decrease of cholesterol levels induced an increase in neurite length and number, while no effect was observed in cortical cells. Interestingly, cultures of hippocampal cells revealed higher levels of cholesterol than the cortical counterparts (Ko et al. 2005). Altogether, it is a provocative idea to consider TRKB as a "sensor" of cholesterol levels in the cell membrane via CARC. Thus, TRKB would trigger synaptic maturation or neurite growth only if the cholesterol levels are ideal for such changes. This assumption, however, remains to be tested.

The insights from the present study could serve as a primary step for experimental testing on the impact of mutations in CRAC/CARC motifs in the TMR of the RTK family. However, we are limited by only considering the role of CRAC/CARC motifs in the TMR of RTKs. Given the promiscuous properties of these motifs, it is plausible to assume multiple false positive CRAC/CARCs in proteins, making data mining and putative *in silico* or *in vitro* analysis difficult to perform. Therefore, more studies focused on refining the algorithms for detecting these motifs are necessary.

Funding

Funding for this study was provided by the ERC (#322742, iPLASTICITY), the EU Joint Programme, Neurodegenerative Disease Research (JPND CircProt #301225), the Academy of Finland (#294710 and #307416), University of Helsinki HiLife Fellowship, the Jane and Eljas Erkko Foundation, and the Sigrid Juselius Foundation.

REFERENCES

Abraham MJ, Murtola T, Schulz R, et al (2015) GROMACS: High performance molecular simulations through multi-level parallelism from laptops to supercomputers. SoftwareX 1-2:19–25

Arnarez C, Uusitalo JJ, Masman MF, et al (2015) Dry Martini, a coarse-grained force field for lipid membrane simulations with implicit solvent. J Chem Theory Comput 11:260–275

Baier CJ, Fantini J, Barrantes FJ (2011) Disclosure of cholesterol recognition motifs in transmembrane domains of the human nicotinic acetylcholine receptor. Sci Rep 1:69

Bekinschtein P, Cammarota M, Medina JH (2014) BDNF and memory processing. Neuropharmacology 76 Pt C:677–683

Bothwell M (2014) NGF, BDNF, NT3, and NT4. Handb Exp Pharmacol 220:3–15

Boyles JK, Pitas RE, Wilson E, et al (1985) Apolipoprotein E associated with astrocytic glia of the central nervous system and with nonmyelinating glia of the peripheral nervous system. J Clin Invest 76:1501–1513

Bussi G, Donadio D, Parrinello M (2007) Canonical sampling through velocity rescaling. J Chem Phys 126:014101

Casarotto PC, Girych M, Fred SM, et al (2019) Antidepressants act by binding to the cholesterol-interaction site at TRKB neurotrophin receptor. bioRxiv 757989

Chaves EIP de, Rusiñol AE, Vance DE, et al (1997) Role of Lipoproteins in the Delivery of Lipids to Axons during Axonal Regeneration. J Biol Chem 272:30766–30773

de Jong DH, Baoukina S, Ingólfsson HI, Marrink SJ (2016) Martini straight: Boosting performance using a shorter cutoff and GPUs. Comput Phys Commun 199:1–7

de Jong DH, Singh G, Bennett WFD, et al (2013) Improved Parameters for the Martini Coarse-Grained Protein Force Field. J Chem Theory Comput 9:687–697

Dekkers MPJ, Nikoletopoulou V, Barde Y-A (2013) Cell biology in neuroscience: Death of developing neurons: new insights and implications for connectivity. J Cell Biol 203:385–393

Dietschy JM, Turley SD (2004) Thematic review series: Brain Lipids. Cholesterol metabolism in the central nervous system during early development and in the mature animal. J Lipid Res 45:1375–1397

Di Scala C, Baier CJ, Evans LS, et al (2017) Chapter One - Relevance of CARC and CRAC Cholesterol-Recognition Motifs in the Nicotinic Acetylcholine Receptor and Other Membrane-Bound Receptors. In: Levitan I (ed) Current Topics in Membranes. Academic Press, pp 3–23

Elkins MR, Sergeyev IV, Hong M (2018) Determining Cholesterol Binding to Membrane Proteins by Cholesterol 13C Labeling in Yeast and Dynamic Nuclear Polarization NMR. J Am Chem Soc 140:15437–15449

Epand RM (2006) Cholesterol and the interaction of proteins with membrane domains. Prog Lipid Res 45:279–294

Fantini J, Barrantes FJ (2013) How cholesterol interacts with membrane proteins: an exploration of cholesterol-binding sites including CRAC, CARC, and tilted domains. Front Physiol 4:31

Fantini J, Di Scala C, Evans LS, et al (2016) A mirror code for protein-cholesterol interactions in the two leaflets of biological membranes. Sci Rep 6:21907

Fantini J, Epand RM, Barrantes FJ (2019) Cholesterol-Recognition Motifs in Membrane Proteins. Adv Exp Med Biol 1135:3–25

Frank C, Rufini S, Tancredi V, et al (2008) Cholesterol depletion inhibits synaptic transmission and synaptic plasticity in rat hippocampus. Exp Neurol 212:407–414

González-González IM, Jaskolski F, Goldberg Y, et al (2012) Measuring membrane protein dynamics in neurons using fluorescence recovery after photobleach. Methods Enzymol 504:127–146

Goritz C, Mauch DH, Pfrieger FW (2005) Multiple mechanisms mediate cholesterol-induced synaptogenesis in a CNS neuron. Mol Cell Neurosci 29:190–201

Hamdan FF, Myers CT, Cossette P, et al (2017) High Rate of Recurrent De Novo Mutations in Developmental and Epileptic Encephalopathies. Am J Hum Genet 101:664–685

Hanson MA, Cherezov V, Griffith MT, et al (2008) A Specific Cholesterol Binding Site Is Established by the 2.8 Å Structure of the Human β2-Adrenergic Receptor. Structure 16:897–905

Harris JS, Epps DE, Davio SR, Kezdy FJ (1995) Evidence for Transbilayer, Tail-to-Tail Cholesterol Dimers in Dipalmitoylglycerophosphocholine Liposomes. Biochemistry 34:3851–3857

Heinrich C, Lähteinen S, Suzuki F, et al (2011) Increase in BDNF-mediated TrkB signaling promotes epileptogenesis in a mouse model of mesial temporal lobe epilepsy. Neurobiol Dis 42:35–47

Hsu P-C, Bruininks BMH, Jefferies D, et al (2017) CHARMM-GUI Martini Maker for modeling and simulation of complex bacterial membranes with lipopolysaccharides. J Comput Chem 38:2354–2363

Huang EJ, Reichardt LF (2001) Neurotrophins: roles in neuronal development and function. Annu Rev Neurosci 24:677–736

Hunte C (2005) Specific protein-lipid interactions in membrane proteins. Biochem Soc Trans 33:938–942

Jamin N, Neumann J-M, Ostuni MA, et al (2005) Characterization of the Cholesterol Recognition Amino Acid Consensus Sequence of the Peripheral-Type Benzodiazepine Receptor. Mol Endocrinol 19:588–594

Jansson ET, Trkulja CL, Ahemaiti A, et al (2013) Effect of cholesterol depletion on the pore dilation of TRPV1. Mol Pain 9:1

Jeong J, McMahon AP (2002) Cholesterol modification of Hedgehog family proteins. J Clin Invest 110:591–596

Källberg M, Wang H, Wang S, et al (2012) Template-based protein structure modeling using the RaptorX web server. Nat Protoc 7:1511–1522

Karpova NN, Pickenhagen A, Lindholm J, et al (2011) Fear erasure in mice requires synergy between antidepressant drugs and extinction training. Science 334:1731–1734

Ko M, Zou K, Minagawa H, et al (2005) Cholesterol-mediated neurite outgrowth is differently regulated between cortical and hippocampal neurons. J Biol Chem 280:42759–42765

Korinek M, Vyklicky V, Borovska J, et al (2015) Cholesterol modulates open probability and desensitization of NMDA receptors. J Physiol 593:2279–2293

Koskinen M, Bertling E, Hotulainen P (2012) Chapter three - Methods to Measure Actin Treadmilling Rate in Dendritic Spines. In: Conn PM (ed) Methods in Enzymology. Academic Press, pp 47–58

Kurzchalia TV, Ward S (2003) Why do worms need cholesterol? Nat Cell Biol 5:684–688

Landrum MJ, Lee JM, Benson M, et al (2018) ClinVar: improving access to variant interpretations and supporting evidence. Nucleic Acids Res 46:D1062–D1067

Lang T, Bruns D, Wenzel D, et al (2001) SNAREs are concentrated in cholesterol-dependent clusters that define docking and fusion sites for exocytosis. EMBO J 20:2202–2213

Lee AG (2004) How lipids affect the activities of integral membrane proteins. Biochim Biophys Acta 1666:62–87
Li H, Papadopoulos V (1998) Peripheral-Type Benzodiazepine Receptor Function in Cholesterol Transport. Identification of a Putative Cholesterol Recognition/Interaction Amino Acid Sequence and Consensus Pattern. Endocrinology 139:4991–4997
Linetti A, Fratangeli A, Taverna E, et al (2010) Cholesterol reduction impairs exocytosis of synaptic vesicles. J Cell Sci 123:595–605
Liu G, Gu B, He X-P, et al (2013) Transient inhibition of TrkB kinase after status epilepticus prevents development of temporal lobe epilepsy. Neuron 79:31–38
Liu J-P, Tang Y, Zhou S, et al (2010) Cholesterol involvement in the pathogenesis of neurodegenerative diseases. Mol Cell Neurosci 43:33–42
Lomize AL, Hage JM, Pogozheva ID (2018) Membranome 2.0: database for proteome-wide profiling of bitopic proteins and their dimers. Bioinformatics 34:1061–1062
Maguire PA, Druse MJ (1989) The influence of cholesterol on synaptic fluidity, dopamine D1 binding and dopamine-stimulated adenylate cyclase. Brain Res Bull 23:69–74
Mann RK, Beachy PA (2000) Cholesterol modification of proteins. Biochim Biophys Acta 1529:188–202
Martin MG, Ahmed T, Korovaichuk A, et al (2014) Constitutive hippocampal cholesterol loss underlies poor cognition in old rodents. EMBO Mol Med 6:902–917
Martin MG, Perga S, Trovò L, et al (2008) Cholesterol Loss Enhances TrkB Signaling in Hippocampal Neurons Aging in Vitro. Mol Biol Cell 19:2101–2112
Martín MG, Pfrieger F, Dotti CG (2014) Cholesterol in brain disease: sometimes determinant and frequently implicated. EMBO Rep 15:1036–1052
Mauch DH, Nägler K, Schumacher S, et al (2001) CNS synaptogenesis promoted by glia-derived cholesterol. Science 294:1354–1357
Maya Vetencourt JF, Sale A, Viegi A, et al (2008) The antidepressant fluoxetine restores plasticity in the adult visual cortex. Science 320:385–388
Michikawa M, Yanagisawa K (1999) Inhibition of Cholesterol Production but Not of Nonsterol Isoprenoid Products Induces Neuronal Cell Death. J Neurochem 72:2278–2285
Mottaz A, David FPA, Veuthey A-L, Yip YL (2010) Easy retrieval of single amino-acid polymorphisms and phenotype information using SwissVar. Bioinformatics 26:851–852
Nieweg K, Schaller H, Pfrieger FW (2009) Marked differences in cholesterol synthesis between neurons and glial cells from postnatal rats. J Neurochem 109:125–134
Nikoletopoulou V, Lickert H, Frade JM, et al (2010) Neurotrophin receptors TrkA and TrkC cause neuronal death whereas TrkB does not. Nature 467:59–63
Niwa YS, Niwa R (2014) Neural control of steroid hormone biosynthesis during development in the fruit fly Drosophila melanogaster. Genes Genet Syst 89:27–34
Páll S, Hess B (2013) A flexible algorithm for calculating pair interactions on SIMD architectures. arXiv [physics.comp-ph]
Park H, Poo M-M (2013) Neurotrophin regulation of neural circuit development and function. Nat Rev Neurosci 14:7–23
Parrinello M, Rahman A (1981) Polymorphic transitions in single crystals: A new molecular dynamics method. J Appl Phys 52:7182
Pereira DB, Chao MV (2007) The tyrosine kinase Fyn determines the localization of TrkB receptors in lipid rafts. J Neurosci 27:4859–4869
Peters M, Katz B, Lev S, et al (2017) Depletion of Membrane Cholesterol Suppresses Drosophila Transient Receptor Potential-Like (TRPL) Channel Activity. Curr Top Membr 80:233–254
Pfrieger FW (2003a) Role of cholesterol in synapse formation and function. Biochimica et Biophysica Acta (BBA) - Biomembranes 1610:271–280
Pfrieger FW (2003b) Outsourcing in the brain: Do neurons depend on cholesterol delivery by astrocytes? Bioessays 25:72–78
Pfrieger FW, Ungerer N (2011) Cholesterol metabolism in neurons and astrocytes. Prog Lipid Res 50:357–371
Prasanna X, Chattopadhyay A, Sengupta D (2014) Cholesterol Modulates the Dimer Interface of the β2-Adrenergic Receptor via Cholesterol Occupancy Sites. Biophys J 106:1290–1300
Prasanna X, Sengupta D, Chattopadhyay A (2016) Cholesterol-dependent Conformational Plasticity in GPCR Dimers. Sci Rep 6:31858
Quan G, Xie C, Dietschy JM, Turley SD (2003) Ontogenesis and regulation of cholesterol metabolism in the central nervous system of the mouse. Developmental Brain Research 146:87–98
Rukmini R, Rawat SS, Biswas SC, Chattopadhyay A (2001) Cholesterol Organization in Membranes at Low Concentrations: Effects of Curvature Stress and Membrane Thickness. Biophys J 81:2122–2134
Sahu MP, Nikkilä O, Lågas S, et al (2019) Culturing primary neurons from rat hippocampus and cortex. Neuronal Signaling 3:NS20180207
Saito K, Dubreuil V, Arai Y, et al (2009) Ablation of cholesterol biosynthesis in neural stem cells increases their VEGF expression and angiogenesis but causes neuron apoptosis. Proceedings of the National Academy of Sciences 106:8350–8355
Suzuki S, Kiyosue K, Hazama S, et al (2007) Brain-Derived Neurotrophic Factor Regulates Cholesterol Metabolism for Synapse Development. Journal of Neuroscience 27:6417–6427
Suzuki S, Numakawa T, Shimazu K, et al (2004) BDNF-induced recruitment of TrkB receptor into neuronal lipid rafts: roles in synaptic modulation. J Cell Biol 167:1205–1215
Tate JG, Bamford S, Jubb HC, et al (2019) COSMIC: the Catalogue Of Somatic Mutations In Cancer. Nucleic Acids Res 47:D941–D947
The UniProt Consortium (2017) UniProt: the universal protein knowledgebase. Nucleic Acids Res 45:D158–D169
Waterhouse AM, Procter JB, Martin DMA, et al (2009) Jalview Version 2--a multiple sequence alignment editor and analysis workbench. Bioinformatics 25:1189–1191
Wendler F, Franch-Marro X, Vincent J-P (2006) How does cholesterol affect the way Hedgehog works? Development 133:3055–3061
Xia Z, Dudek H, Miranti CK, Greenberg ME (1996) Calcium influx via the NMDA receptor induces immediate early gene transcription by a MAP kinase/ERK-dependent mechanism. J Neurosci 16:5425–5436
Yeo GSH, Connie Hung C-C, Rochford J, et al (2004) A de novo mutation affecting human TrkB associated with severe obesity and developmental delay. Nat Neurosci 7:1187–1189
Zonta B, Minichiello L (2013) Synaptic membrane rafts: traffic lights for local neurotrophin signaling? Front Synaptic Neurosci 5.: https://doi.org/10.3389/fnsyn.2013.00009

FIGURES AND TABLES

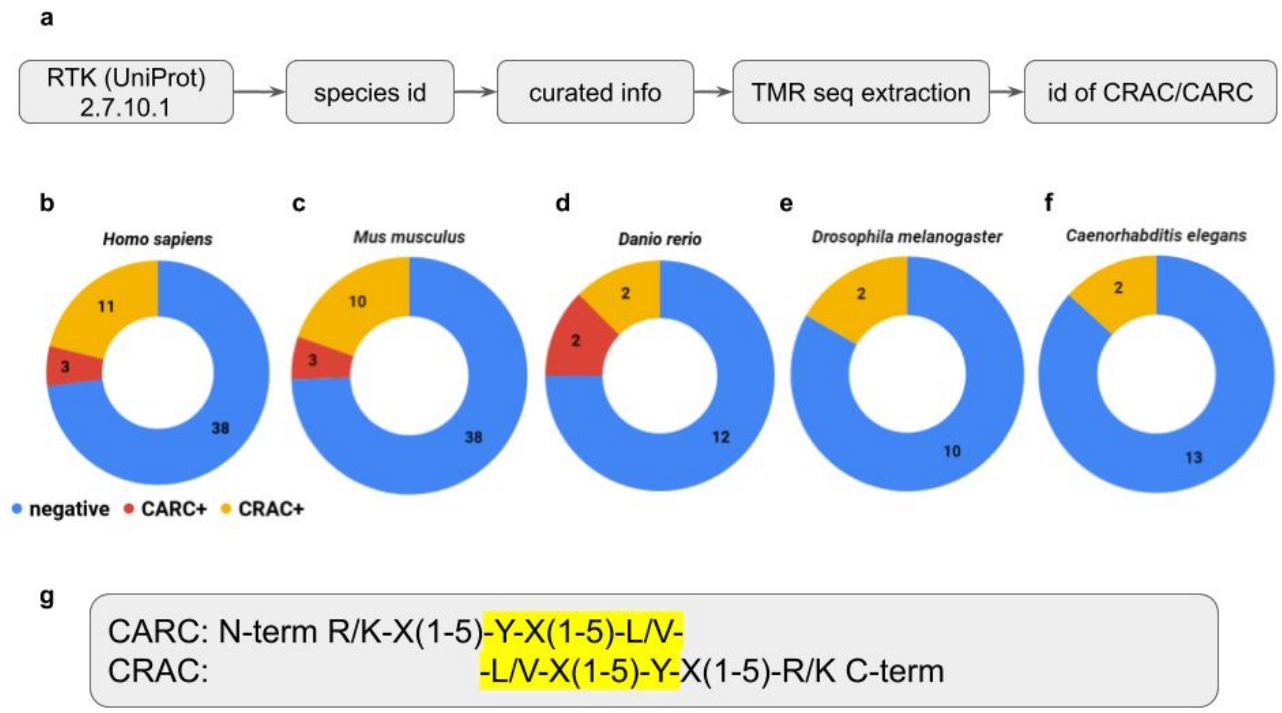

Figure 1. (a) Workflow of data mining. The TMR (transmembrane sequence +5 amino acid residues from each N- and C-terminal sides) of curated entries found in UniProt using the code for tyrosine kinase receptor family (2.7.10.1) were blasted against the library of cholesterol recognition and alignment consensus combinations. The incidence of CRAC and CARC motifs in (b) human, (c) mouse, (d) zebrafish, (e) fruit fly, and (f) *C. elegans* TMR of RTK family members. (g) Library of CRAC and CARC sequences (all combinations used can be found in the stored data). The yellow highlighted region of the sequences must be embedded into the cell membrane.

Table 1. CRAC and CARC(underlined)-positive proteins

Unipro ID	Protein name	Mutation in CRAC/CARC
H. sapiens		
Q9UM73	ALK tyrosine kinase receptor	
Q16620	BDNF/NT-3 growth factors receptor	Y434C
P29320	Ephrin type-A receptor 3	I564V
P11362	Fibroblast growth factor receptor 1	
P22455	Fibroblast growth factor receptor 4	
P08069	Insulin-like growth factor 1 receptor	
P06213	Insulin receptor	F978Y
P07333	Macrophage colony-stimulating factor 1 receptor	L536V, Y540S, K541T, K543M
P10721	Mast/stem cell growth factor receptor Kit	
O15146	Muscle, skeletal receptor tyrosine-protein kinase	
Q15303	Receptor tyrosine-protein kinase erbB-4	
Q12866	Tyrosine-protein kinase Mer	I518V
Q01974	Tyrosine-protein kinase receptor ROR2	
P34925	Tyrosine-protein kinase RYK	
M. musculus		
P97793	ALK tyrosine kinase receptor	
P15209	BDNF/NT-3 growth factors receptor	
Q60750	Ephrin type-A receptor 1	
P29319	Ephrin type-A receptor 3	
P16092	Fibroblast growth factor receptor 1	
Q03142	Fibroblast growth factor receptor 4	
P15208	Insulin receptor	
Q60751	Insulin-like growth factor 1 receptor	
P09581	Macrophage colony-stimulating factor 1 receptor	
P05532	Mast/stem cell growth factor receptor Kit	
Q61006	Muscle, skeletal receptor tyrosine-protein kinase	
Q9Z138	Tyrosine-protein kinase transmembrane receptor ROR2	
Q01887	Tyrosine-protein kinase RYK	
D. rerio		
Q9I8N6	Macrophage colony-stimulating factor 1 receptor	
Q8JFR5	Mast/stem cell growth factor receptor kita	
B8JLJ1	Tyrosine-protein kinase receptor (Ntrk2a)	
A0A0R4ILA2	Tyrosine-protein kinase receptor (Ntrk2b)	
D. melanogaster		
P09208	Insulin-like receptor	
P83097	Putative tyrosine-protein kinase Wsck	
C. elegans		
P34891	Receptor-like tyrosine-protein kinase kin-15	
G5EGK5	Tyrosine-protein kinase receptor cam-1	

a

UniProt ID	NTRK2	human	chimpanzee	mouse	rat	dog	chicken	zebrafish
Q16620	human		100.00	93.92	93.55	98.30	77.13	60.43
A0A2J8MRP9	chimpanzee	100.00		93.92	93.55	98.30	77.13	60.43
P15209	mouse	91.18	91.18		98.54	93.80	76.49	60.39
Q63604	rat	94.12	94.12	97.06		93.55	76.49	60.15
E2RKA1	dog	97.06	97.06	94.12	91.18		77.49	60.68
Q91987	chicken	41.18	41.18	44.12	44.12	41.18		61.09
A0A0R4ILA2	zebrafish 2b	35.29	35.29	35.29	35.29	35.29	50.00	

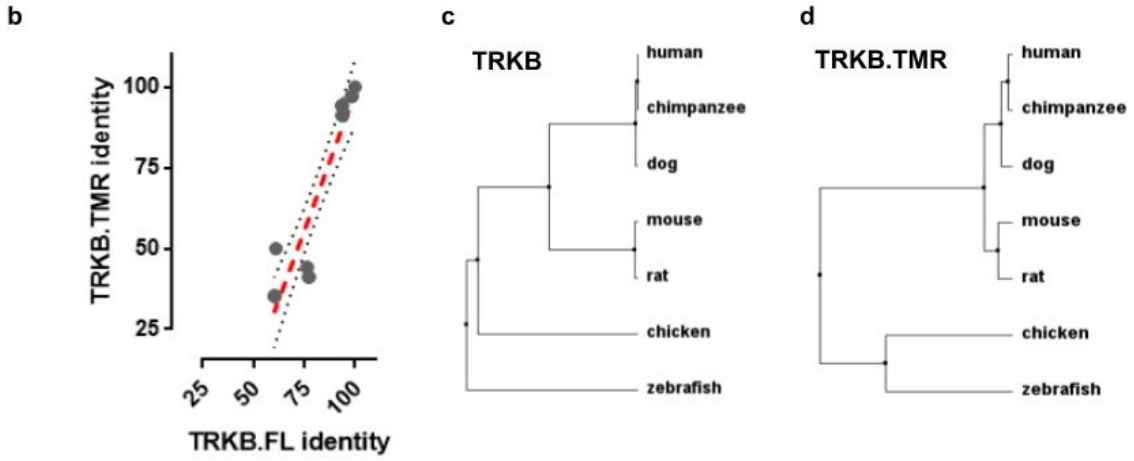

Figure 2. (a) Percent identity (PI) for full length (red) and TMR (green) of TRKB. The amino acid sequence of full length and TMR of TRKB (NTRK2) from different species were verified for PI in UniProt database. (b) Correlation between the PI in full length and TMR of TRKB [Spearman's test. R^2= 0.8530; 99%CI= 0.7564 to 0.9775; p<0.0001]; dashed line= 99% confidence band. PI tree of (c) full length and (d) TMR of TRKB.

Table 2. CARC-containing sequences (red) in TRKB.TMR among vertebrate species.

UniProt	Species	TMR sequence
Q16620	*H. sapiens*	TGREHLSVYAVVVIASVVGFCLLVMLFLLKLARH
A0A2J8MRP9	*P. troglodites*	TGREHLSVYAVVVIASVVGFCLLVMLFLLKLARH
P15209	*M. musculus*	SNREHLSVYAVVVIASVVGFCLLVMLLLLKLARH
Q63604	*R. norvegicus*	TNREHLSVYAVVVIASVVGFCLLVMLLLLKLARH
E2RKA1	*C. familiaris*	SGREHLSVYAVVVIASVVGFCLLVMLFLLKLARH
Q91987	*G. gallus*	ENEDSITVYVVVGIAALVCTGLVIMLIILKFGRH
A0A0R4ILA2	*D. rerio*	PLEDRVAVYIVVGIAGVALTGCILMLVFLKYGRS

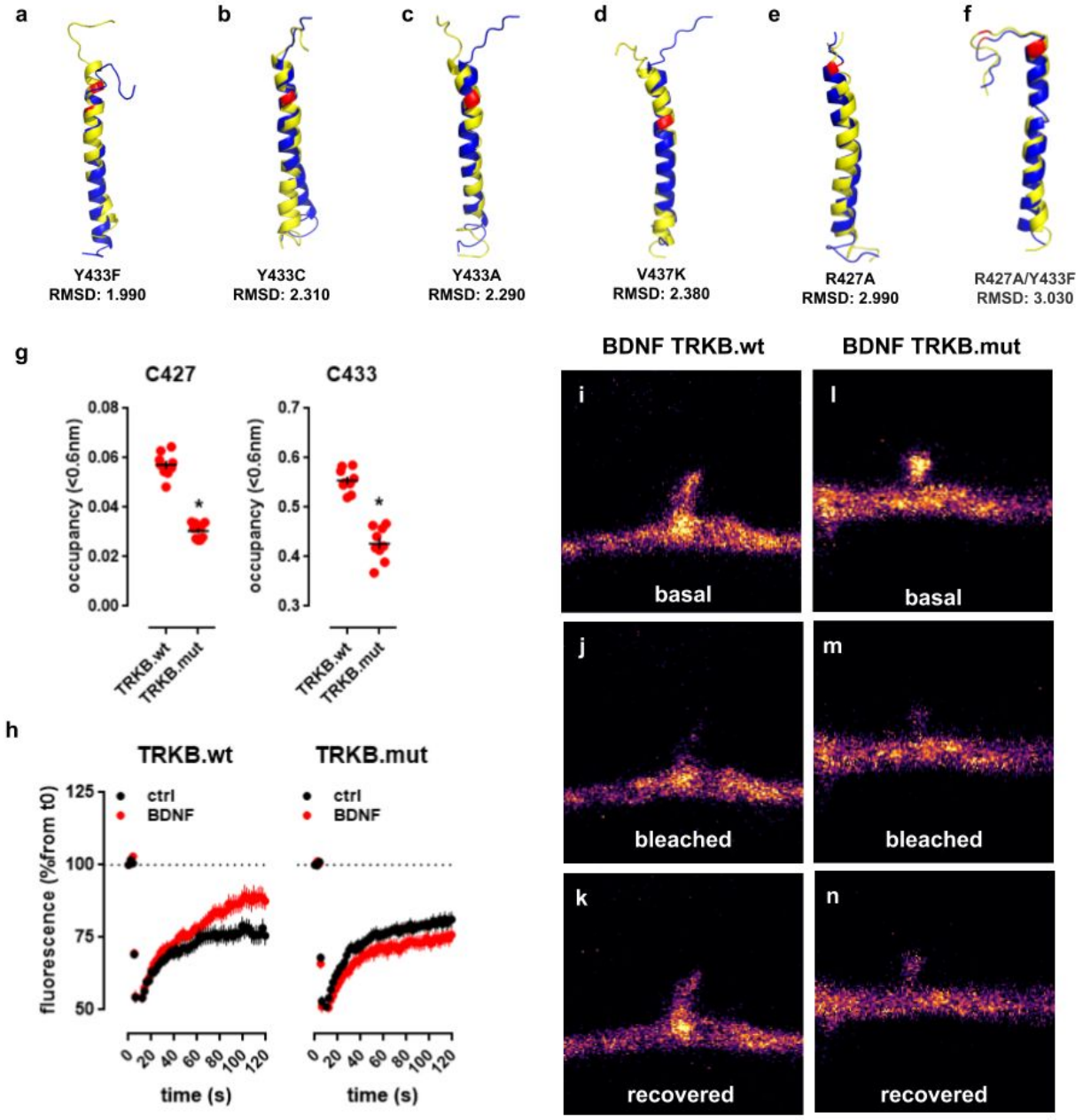

Figure 3. The amino acid sequences of mouse TRKB TMR (wild-type and carrying a point mutation the CARC motif) were submitted to RaptorX server. The alignment of mutant models against wild-type TMR with the root mean squared deviation (RMSD, values expressed in Å) between the atoms in the backbone of the chains for (a) Y433F, (b) Y433C, (c) Y433A, (d) V437K, (e) R427A, and (f) R427A/Y433F mutations. Yellow: TMR of wild-type; blue: TMR of mutant; red: site of mutation. (g) The R427A/Y433F mutation compromised the interaction between the TRKB CARC motif and cholesterol at C-alpha in R427 and Y433 residues by coarse-grained molecular dynamics simulations. (h) Treatment with BDNF (20ng/ml/15min) induced a recovery in the spine fluorescence, and the mutation of TRKB CARC motif compromises the BDNF-induced movement of GFP-tagged TRKB. (i-n) Fluorescence observed in cultured hippocampal cells from rat embryo (E18, DIV 16-18), before, immediately, and 2 min after bleaching (recovered) (c-h). *$p<0.05$ from control (TRKB.wt).